

## State variables estimation and riparian vegetation species mapping for the Negro river, Spain, by hyperspectral imaging.

Peña MA.\*

[marco.pena@umayor.cl](mailto:marco.pena@umayor.cl)

Cruz P.C.\*

[pablo.cruzj@umayor.cl](mailto:pablo.cruzj@umayor.cl)

Castro B.P.\*

[benjamin.castro@umayor.cl](mailto:benjamin.castro@umayor.cl)

\*Centro de Estudio de Recursos Naturales Oterra

**Resumen:** En este trabajo exploramos las capacidades que ofrece la teledetección hiperespectral aérea para estimar turbidez y profundidad del agua, y para mapear especies de vegetación ripariana en el río Negro, España. Datos de campo de ambas variables y localidades representativas de las principales especies arbóreas de vegetación fueron colectadas al mismo momento de adquirir los datos remotos. Fueron llevadas a cabo correlaciones entre ambos conjuntos de datos para encontrar el índice de diferencia normalizada (IDN) que mejor relaciona cada variable de estado. Un clasificador hiperespectral supervisado, entrenado con datos de campo, fue usado para mapear la distribución de las especies arbóreas. Los resultados muestran que el mejor seguimiento de los cambios de profundidad del agua se consigue con un IDN construido con la banda del infrarrojo cercano (IC) de 705,5 nm y la banda verde del visible de 531,1 nm ( $r = 0.69$ ). En tanto, el mejor seguimiento de los cambios de turbidez del agua se consigue con un IDN construido con las bandas IC de 905,34 nm y de 760 o 774,54 nm ( $r = 0.82$ ). Ambos resultados fueron encontrados consistentes con el acervo teórico existente. La inspección visual de la imagen de salida entregada por el algoritmo de clasificación sugiere que la teledetección hiperespectral es alentadora para mapear especies de vegetación ripariana. A futuro, se espera que la metodología empleada en este trabajo sea mejorada, de manera de proveer una validación sólida que apoye el uso de esta tecnología en otros cuerpos de agua del país.

**Abstract:** In this work we explore the capacities that airborne hyperspectral imaging offers to estimate water's turbidity and depth, and to map riparian vegetation species in the Negro river, Spain. Ground based data of both state variables, and representative locations of the main tree vegetation species were collected at the same time of the remotely sensed data acquisition. Correlations were carried out between both data sets in order to find the normalized difference index (NDI) that best relates each state variable. A supervised hyperspectral classifier, trained with field data, was used to map the distribution of the tree species. Results show that water's depth changes are best tracked by a NDI constructed with the near infrared (NIR) band at 705.5 nm and a green visible band at 531.1 nm ( $r = 0.69$ ). Meanwhile, water's turbidity changes are best tracked by a NDI constructed with the near infrared bands at 905.34 nm, and at 760 or 774.54 nm ( $r = 0.82$ ). Both results were found to be consistent with the theoretical background. The visual inspection of the output image rendered by the classification algorithm suggests that hyperspectral imaging is encouraging for the riparian vegetation species mapping. An improvement of the methodology employed in this work is expected in the future, in order to provide a solid validation that supports the use of this technology in other water bodies of the country.

Keywords: hyperspectral imaging spectral indices, riparian vegetation, water turbidity, water depth

## 1. Introduction

Optical hyperspectral remote sensing is a scientific discipline that retrieves information from an element by detecting and analyzing its radiated energy throughout hundreds of spectral samplings (from now bands) continuously located in the visible and infrared dimensions of the electromagnetic spectrum (i.e., optical spectral range). In specific spectral wavelengths of that range most of the biotic and abiotic elements of the Earth surface produce absorption and reflection features that allow their physical and chemical characterization. Nevertheless, only remote sensors with hyperspectral sensitivity can properly measure the wide range of those signals (Lucas *et al.*, 2004; Borengasser *et al.*, 2008; Goetz, 2009).

Optical remote sensing has largely assisted the study of water resources, mainly by estimating and predicting water quality parameters such as turbidity, dissolved organic matter and algae concentration (Govender *et al.*, 1999; Ritchie *et al.*, 2003). In the optical spectral range sediments and microorganisms contained in a water body produce distinctive signals that can be isolated by the design of spectral indices, or arithmetic combinations of bands sensitive to the presence of a biogeochemical compound. The strength of a spectral index relies on its simple formulation (usually it combines a band sensitive to the compound variations and another one insensitive to it, that serves as baseline) and its capacity of minimize factors that may interferes in the measured compound (e.g, solar illumination and sensor viewing geometry, scattered path radiance, signals from other elements contained within the pixel) (Treitz and Howarth, 1999; Asner *et al.*, 2003; Liang, 2004; Blackburn, 2007).

The remotely sensed assessment of state variables of a water body can be drastically improved by using hyperspectral images with high spatial resolution (i.e., hyperspatial) acquired from airborne platforms, because they allow to track them with unprecedented spectral and spatial detail, and throughout specific temporal windows. This work explores the capacities that this type of images offer for estimating water's turbidity and depth, as well as for mapping riparian vegetation species in the Negro river, Zamora district, Spain. The river forms part of the Duero basin, located at the northwest of the Spanish territory. Their waters are calm, shallow and very clear. The study area comprises a river transect of about 18 km, from the Agavanzal reservoir (41°58' N 6°12' W) to the Dornillas locality (42°03' N 6°19' W), approximately. Hyperspectral images were acquired at the same time of field data collection. Statistical analyses were performed between both data sets in order to find the empirical spectral indices that best relate the state variables of interest. Thereafter, supervised classification procedures were applied on the images in an attempt to map the vegetation species of interest.

## 2. Methods

*Image acquisition:* Hyperspectral images were acquired by an optical imaging spectroradiometer. Specifically, a Hypspx VNIR 1600© hyperspectral line scanner was used, which is sensitive to wavelengths comprised between 400 and 1000 nm of the electromagnetic spectrum (i.e., visible and near infrared regions). This range is sampled at 3.7 nm intervals, thus providing a spectral resolution of 160 bands. Each band records a dynamic range of 65,536 voltage levels, which means a radiometric resolution or digitization of 16 bit. The scanner's field of view (FOV) is 17°, across which a linear array of 1,600 voltage detectors (Charge Coupled Device, CCD) scans the surface with an instantaneous field of view (IFOV) of 0.185 and 0.37 mrad in the across track and along track direction, respectively. The geographic positioning of the scanned lines is achieved by an IMAR iTrace RTF200© inertial measurement unit (IMU) or inertial navigation system (INS), that simultaneously reads the aircraft attitude and tilt, and the geographic coordinates of the swapped terrain, with a frequency of 0.005 s. Images were acquired from a Cessna 402 aircraft on October 29, 2009, between 3 and 4 pm, local hour. The flight was made at a constant speed and altitude above ground of 296 km/h and 1,200 m, respectively. During the flight atmosphere was stable, sky was clear and the solar elevation fluctuated from 29 to 28° approximately. For the flight date, the lowest solar zenith angle of the study area occurs around 1 pm, local hour ( 57°). Therefore, in spite of the flatness of the swapped terrain relief, the acquisition of images out of the

maximum solar elevation contributed to increase the presence of superficial shadows (particularly those projected by trees).

*Image pre-processing:* Original digital numbers (DNs) recorded on the image's pixels were automatically converted into absolute radiances by using the scanner's radiometric exportation software. Though ideally at sensor radiances should be converted into apparent surface reflectances (i.e., the ratio of irradiance to radiance, both free of atmospheric effects), the image's atmospheric correction cannot be performed because during the period of this study the software considered for this purpose (ATCOR®, Atmospheric Correction) was being tested. Nonetheless, calibrated radiances were considered suitable for the achievement of the study goals (RSI, 2009; Liang, 2004).

Image's geometric correction was performed by using PARGE® (Parametric Geocoding) software, which is specially designed for the correction of airborne hyperspectral imagery. For its operation, the software requires the aircraft attitude data (i.e., roll, pitch and yaw), the geographic coordinates of the scanned lines and a digital elevation model (DEM) of the study area. Spatial resampling of the scenes was made at 0.45 m (i.e., the along track pixel dimension) by using the bilinear interpolation method. Compared with the traditional nearest neighbour resampling, bilinear interpolation renders an image with a better geometry but at the expense of altering the original pixel radiometry. This is because the radiometric value that is assigned to the corrected pixel results from a distance weighted average of the radiance values of their four nearest uncorrected pixels. Nonetheless, this radiometric smoothness was considered as positive, since contributed to minimize spatial mismatches that subsequently could arise between field sampled plots and their corresponding image pixels, as a result of geographic coordinate inaccuracies on each data set. The geographic coordinates system assigned to the output images was UTM (Universal Transverse of Mercator), datum WGS84 (World Geodetic System 1984), zone 29, North. Finally, an images' mosaic was constructed, which subsequently was trimmed according to a distance of 250 m from the river shoreline with the sense of only submitting to later processing the interest area.

*Field data collection:* Field campaign was carried out at the same time of the flight, with the sense of minimizing the negative effect that any temporal variability in the compounds of the measured variables may have in the later statistical analysis accomplished between ground based data (physical units of the variable) and remotely sensed data (pixel radiances). The first task consisted in the identification of tree species within three spatial windows that were defined at regular intervals along the studied river's transect. The species identified were: Chopo blanco/Chopo negro (*Populus alba/Populus nigra*), Aliso (*Alnus glutinosa*), Encino (*Quercus ilex*), Roble (*Quercus pyrenaica*), and Pino (*Pinus pinaster*). All these species were marked as plots on a high spatial resolution cartography of the study area by field personnel. Afterward, inside each window water turbidity (nephelometric turbidity units, NTU) and water depth (m) were measured on 23 plots each one, in order to statistically relate these data with their corresponding pixel radiances. Plots were selected according to an *ad-hoc* sampling method and the measurements were accomplished by using a zodiac boat, preferably moved by oars in order to not disturb the sampled waters. To minimize the confusion that water depth may introduce in the water turbidity analysis, all the turbidity plots were sampled on areas with a similar depth. By the same token, water depth was sampled on areas with similar turbidity. Finally, with the purpose of minimizing spatial coregister inconsistencies between field sampled plots and their corresponding image pixels, all the measurements were carried out by considering a plot's support region of about 2 m of diameter. Geographic coordinates of the field data were collected by a geodetic GPS (Global Positioning System), set to a positional accuracy below 0.5 m.

*Supervised classification:* Field sampled plots of the tree species were superimposed on the image (i.e., trimmed images mosaic) to define training areas corresponding to each species. Additionally, training areas corresponding to other elements such as water, bare soils, impervious surfaces, rooftops and grasslands were also defined. The statistical separability between the spectral curves of all pairs of the interest elements (from now classes) was determined through the Divergence Transformed measure. In all cases, a high separability ( $\cong 2,000$ , the maximum possible divergence value) was retrieved. For the mapping purpose, the Spectral Angle Mapper (SAM) was used. This is a hyperspectral classification algorithm that assigns each image pixel to a given class based on their spectral similarities. Specifically,

the algorithm calculates the angular distance (in radians) between the spectral curve of each pixel and a given class, assigning the pixel to the class which more resembles. Though the algorithm can operate with a threshold from which a pixel will not be classified, we decided to force the classification of all pixels, mainly because of our uncertainty in the spectral variability that each class may comprise. Ideally, an image classification process should end with an accuracy assessment based on a contingency table (i.e., the comparison of each class with their corresponding ground truth data). Nonetheless, this procedure was beyond the study scope. So, we recognize that no quantitative approach was attempted for such an evaluation, but just a simple visual inspection based on the knowledge of the study area.

*Empirical spectral indices retrieval:* Field sampled plots of water turbidity and depth were superimposed on the image for extracting their corresponding pixel radiance values. Afterward, each parameter was correlated to the radiances resulting from a normalized difference index (NDI).

$$(L\lambda_1 - L\lambda_2) / (L\lambda_1 + L\lambda_2) \quad (1)$$

Where  $L\lambda_1$  and  $L\lambda_2$  are the absolute radiances of two image bands. We first found the band that best correlates their corresponding field data, and that was the  $L\lambda_1$  formula term. Then, each one of the remaining bands were entered in the formula as the  $L\lambda_2$  term, and new correlations were retrieved. By doing this step, we obtained the NDI that best tracks a given parameter. Pearson correlations were used for water depth field data. Since the distribution of water turbidity field data was not normal, Spearman correlations were used.

### 3. Results and discussion

*Spectral behaviour of riparian vegetation species:* As it is well known, the typical spectral behaviour (i.e., spectral pattern) of healthy vegetation is characterized by a high reflection in the green visible region (500 600 nm) and a strong absorption in the red visible region (600 700 nm), mainly due to the presence of foliar chlorophyll pigments (major responsables of vegetation's photosynthesis). Meanwhile, in the near infrared (NIR) region (700 1,000 nm) a very high reflection occurs as a result of the presence of healthy leaves, except for the spectral range between 900 and 970 nm, where absorption features are due to the leaf water content (Peñuelas *et al.*, 1993, 1997; Asner, 1998, 2003; Treitz and Howarth, 1999; Liang, 2004; McCoy, 2005). These spectral signals are clearly distinguishable in figure 1a, which shows the spectral curves retrieved from the tree species sampled in the field. However, they are some differences between them. The spectral curve of Chopo class stands out for its highest reflection in the green and red visible regions. It also shows a high reflection in the NIR region, that only is overcome by the grassland class. Therefore, though its chlorophyll related absorption is not stronger than the remaining species, its reflection due to the foliage abundance is one of the highest. It is likely that this spectral behaviour is due to structural characteristics or foliar attributes of the species, that favours the radiation reflection (e.g., LAD directs most of the incident radiation to the sensor view or radiative properties of leaves, such as colour and texture, favour a high reflection). It is unlikely to attribute that spectral behaviour to some particularity related to the species' condition, mainly because if its absorption is relatively low in the red visible region, it should be expected that its reflection be also relatively low in the NIR region, which does not happen. This does happen with the grassland class, which evidences the high cover and health status of that physiognomic type. In general, spectral curves of the sampled tree species exhibit their larger separation in the NIR region, that usually has been referred to as the spectral region that most contributes to the species discrimination, because of their sensitivity to the vegetation canopy structure attributes, which can reach notorious differences among species (Asner, 1998; Liang, 2004; McCoy, 2005). Figure 1b shows the typical spectral behaviour of clear water, which is characterized by a very low reflection in the whole visible region and an almost complete absorption in the NIR region (Lillesand *et al.*, 2004; McCoy, 2005). Meanwhile, bare soil classes present a regular and relatively high reflection on those spectral

regions. Spectral curves from vegetation as well as from the remaining elements show strong absorption features between 760 and 940 nm of the spectrum, which are due to oxygen and water vapour content in the atmosphere, respectively (Schläpfer *et al.*, 1998, 2005; Teillet *et al.*, 1998; Richter, 2010). These spectral signals are specially notorious when at sensor radiances are used, since the scattered path radiance has not been compensated and spectral irradiance has not been considered.

*Mapping of riparian vegetation species:* Figure 2 shows a representative spatial window of the vegetation species classified across the riparian zone of the Negro river. During the training area stage, no attempt was made to identify shadowed features, since they could comprise a wide spectral variability (according to their intensity and the land cover type that they cover) that may confuse the algorithm's class assignment, thus promoting the image misclassification. In other words, it was the algorithm who assigned shadowed features to the class that more resembles. As a result, most of them were classified as bare soils. Due to their spectral similarity, some shallow waters were confounded with bare soils. Regarding vegetation classification performance, Aliso class tends to be identified across the river shoreline, though in some cases it is confounded by Roble and Encina classes. Chopo and Roble canopies exhibit quite distinguishable visual appearances, so it was easy to check if they were correctly classified. A visual inspection suggests that both classes were classified with high accuracy. There are many cases in which a single tree canopy shows more than one class. This evidences the spectral complexity that vegetation species may achieve, and highlights the need of a more representative and accurate selection of the training areas, in such a way that these misclassifications be minimized. At this point, it is important bearing in mind that the spectral behaviour of vegetation results from a combination of phenological, physiological, physiognomic and site specific factors. According to this, a given vegetation species class might be divided into several subclasses, even within a relatively small and apparently homogenous study area.

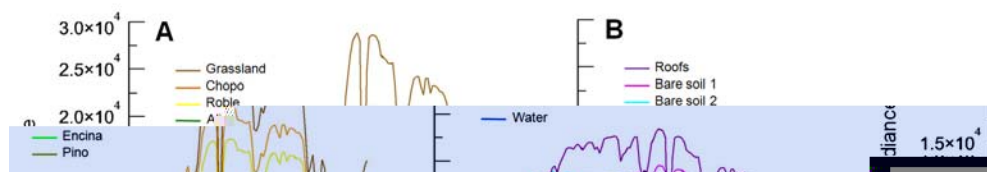


Figure 1. Spectral curves of vegetation species (A) and other elements (B) of interest extracted from the hyperspectral data.

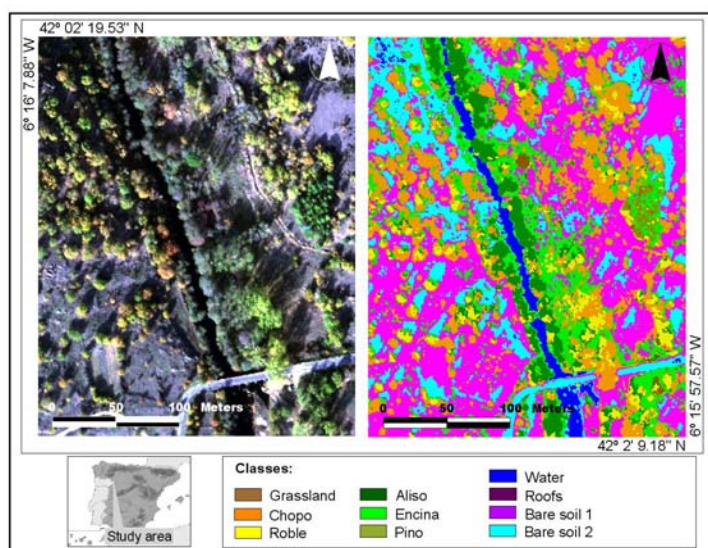


Figure 2. Vegetation species mapping for a spatial window of the study area.

*Water's depth and turbidity indices:* Figure 3a allows us to observe the bands significantly correlated to water depth. The highest correlations were found for NIR bands with central wavelengths at 705.5 nm (band 82), 709.14 nm (band 83), 701.87 nm (band 81), 712.77 nm (band 84) and 720.03 nm (band 86) ( $r = 0.69; 0.69; 0.68; 0.67; 0.67$ , respectively). It is likely that these spectral wavelengths are sensitive to changes in the amount of suspended sediment contained throughout the water column, which indirectly are related to water depth (if water depth increases then suspended sediments should also increase). According to figure 3b the NDI that best correlates water depth ( $r = 0.75$ )

E

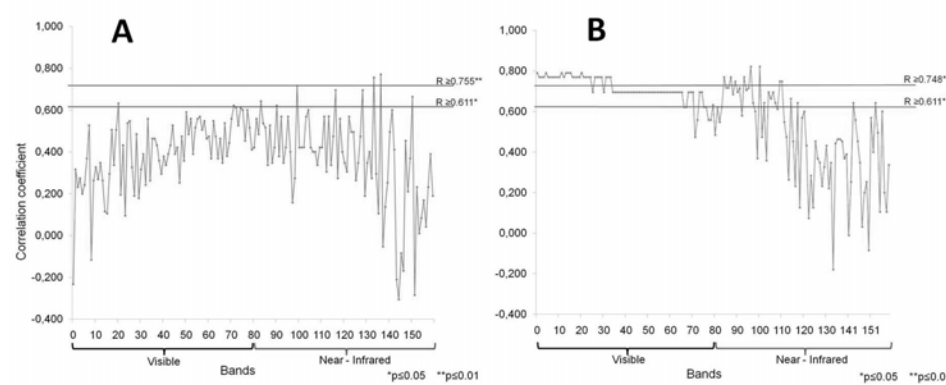


Figure 4. Correlations for hyperspectral bands and water's turbidity (A), and for NDI and water's turbidity (B).

#### 4. Conclusions

This work explored the capacities that optical hyperspectral remote sensing offers for estimating water state variables and for mapping riparian vegetation species in the Negro River, Spain. The results support the potential of this technology to accomplish aims as the pursued in this work. Empirical statistical analysis show that it is possible to design spectral indices closely related to water's turbidity and depth changes. Meanwhile, an encouraging discrimination of vegetation species may be derived from this type of images if appropriately representative spectral curves may be extracted from the targets of interest.

From the experience gained in this work, some methodological enhancements are recommended for similar future applications of this technology. First, it would be desirable to minimize the atmosphere induced effects on the image data. Even when scattered path radiance should be low for images acquired near the ground (mainly because of to the low optical thickness of the atmosphere), the use of atmospherically corrected radiometric units (i.e., surface reflectances) would provide more reliability and validity to the results obtained. Second, in spite of the expensive that it can be to increase the number of field sampled plots, it would be recommendable to procure the highest number possible in order to minimize potential overfitting problems in the subsequent statistical analysis. Third, a classification's accuracy assessment should be accomplished at least over sensible or representative areas, in order to provide a quantitative measure of the degree of success achieved by the supervised classification procedure.

#### References

Aronoff S. 2005. *Remote Sensing for GIS Managers*. ESRI Press. New York, USA. 487 p.

Asner G.P. 1998. Biophysical and biochemical sources of variability in canopy reflectance. *Remote Sensing of Environment*, 64: 234-253.

Asner G., Hicke J., Lobell D. 2003. Per pixel analysis of forest structure: Vegetation indices, spectral mixture analysis and canopy reflectance modeling. In Wulder MA., Franklin S.E. eds. *Remote Sensing of Forest Environments: Concepts and Case Studies*. Kluwer Academic Publishers. Dordrecht, Holland. p. 209-254.

Bhargava D.S., Mariam D.W. 1991. Light penetration depth, turbidity and reflectance related relationships and models. *ISPRS Journal of Photogrammetry and Remote Sensing*, 46: 217-230.

Blackburn G.A. 2007. Hyperspectral remote sensing of plant pigments. *Journal of Experimental Botany*, 58(4): 855 867.

Borengasser M, Hungate W.S., Watkins R. 2008. *Hyperspectral Remote Sensing, Principles and Applications*. CRC Press. Florida, USA. 119 p.

Doxaran D., Froidefond JM, Lavender S., Castaing P. 2002a. Spectral signature of highly turbid water. Application with SPOT data quantify suspended particulate matter concentrations. *Remote Sensing of Environment*, 81: 149 161.

Doxaran D., Froidefond JM, Lavender S., Castaing P. 2002b. A reflectance band ratio used to estimate suspended matter concentrations in sediment dominated coastal waters. *International Journal of Remote Sensing*, 23(23): 5079 5085.

Goetz A.F.H. 2009. Three decades of hyperspectral remote sensing of the Earth: A personal view. *Remote Sensing of Environment*, 113: S5 S16.

Govender M, Chetty K, Bulcock H. 2007. A review of hyperspectral remote sensing and its application in vegetation and water resource studies. *Water SA*, 33(2): 145 152.

Liang S. 2004. *Quantitative Remote Sensing of Land Surfaces*. Wiley. New Jersey, USA. 560 p.

Lillesand T.M, Kiefer R.W., Chipman J.W. 2004. *Remote Sensing and Image Interpretation*. Wiley. New York, USA. 763 p.

Lucas R., Rowlands A, Niemann O, Merton R. 2004. Hyperspectral sensors and applications. In Varshney P.K, Arora MK. eds. *Advanced Image Processing Techniques for Remotely Sensed Hyperspectral Data*. Berlin, Germany. Springer. p. 11 49.

McCoy R.M. 2005. *Field Methods in Remote Sensing*. The Guilford Press. New York, USA. 159 p.

Peñuelas J, Fillela I, Biel C, Serrano L, Savé R. 1993. The reflectance at the 950 970 nm region as an indicator of plant water status. *International Journal of Remote Sensing*, 14(10): 1887 1905.

Peñuelas J, Peñol J, Ogaya R, Fillela C. 1997. Estimation of plant water concentration by the reflectance Water Index WI (R900/R970). *International Journal of Remote Sensing*, 18(13): 2869 2875.

Richter R. 2010. *Atmospheric/Topographic Correction for Airborne Imagery*. German Aerospace Center. Wessling Germany. 157 p.

Ritchie J.C., Zimba P.V., Everitt J. H. 2003. Remote sensing techniques to assess water quality. *Photogrammetric Engineering and Remote Sensing*, 69(6): 695-704.

RSI (Research Systems Incorporation). 2009. *ENVI (Environment for Visualizing Images) Online Help*. ITT Visual Information Solutions. Boulder, USA. (unpaginated).

Schläpfer D., Borel C.C., Keller J., Itten K.I. 1998. Atmospheric pre corrected differential absorption techniques to retrieve columnar water vapour. *Remote Sensing of Environment*, 65(3): 353-366.

Schläpfer D., McCubbin I.B., Kindel B., Kaiser J.W., Ben Dor E. 2005. Wildfire smoke analysis using the 760 nm oxygen absorption feature. *In proceedings of the 4<sup>th</sup> EARSeL Workshop on Imaging Spectroscopy*. April 27 - 29. Warsaw University. Warsaw, Poland. 10p.

Teillet P.M., Staenz K., Williams D.J. 1997. Effects of spectral, spatial, and radiometric characteristics on remote sensing vegetation indices of forested regions. *Remote Sensing of Environment*, 61: 139-149.

Treitz P.M., Howarth P.J. 1999. Hyperspectral remote sensing for estimating biophysical parameters of forest ecosystems. *Progress in Physical Geography*, 23(3): 359-390.